

CFD Modelling for Recalcitrant Aldehyde Oxidations in VUV/UV Photoreactors

Hongjun Ye^{1,2}, Xiaodong Ruan^{1,2}, Rui Su^{*1,2}, Yingnan Shen^{1,2}, Jing Wang^{1,2}, Liang Hu^{1,2}

¹ State Key Laboratory of Fluid Power and Mechatronic Systems, Zhejiang University

² Engineering Research Center of DLIS, Ministry of Education

Zhejiang University, Hangzhou, China;

12225022@zju.edu.cn; xdruan@zju.edu.cn; srhello@zju.edu.cn;

shenyngnan@zju.edu.cn; jing.wang@zju.edu.cn; cmeehuli@zju.edu.cn

Abstract - This study presents a CFD model to investigate the degradation behaviour of the recalcitrant aldehyde in the VUV/UV photoreactor, with a focus on hydrodynamics, radical generation, and oxidation processes. The evaluation of photoreactor performance considers the impact of degradation and formation behaviour of primary and secondary pollutants. Results indicate a strong positive correlation between 185 nm VUV irradiance and OH· radical generation. Acetaldehyde is rapidly degraded along the reactor, which has been almost completely removed by the midpoint. However, secondary organic contaminants, such as formic and acetic acids, impede complete mineralization, leading to a 24% reduction in total organic carbon at the outlet. The influence of hydrodynamics, including vortex generation and velocity profiles, on the spatial distribution of both primary and secondary contaminants is analysed, with a comparison of five RANS models. These findings provide valuable insights into optimizing reactor performance for effective contaminant degradation and mineralization.

Keywords: CFD; VUV/UV photoreactor; Degradation of aldehyde; Hydrodynamics

1. Introduction

Ultrapure water (UPW) is an essential resource for the electronics industry, extensively utilized in semiconductor manufacturing processes such as cleaning, reagent preparation, immersion lithography, and cooling. The semiconductor industry imposes strict requirements on the organic contaminants in UPW, specifically on the total organic carbon (TOC) content (at ppb level)[1–3]. UV irradiation has become a widely adopted technique in water treatment [4], while UV-based advanced oxidation processes (AOPs), such as UV/H₂O₂ and UV/TiO₂, are extensively applied in contaminants degradation [5]. Vacuum ultraviolet/ ultraviolet (VUV/UV) treatment, considered a highly promising method due to its significant advantage of operating without additional chemical inputs, is predominantly implemented during the polishing stage, aiming to efficiently remove bacteria and organic compounds [3, 6].

In the past few decades, Computational fluid dynamics (CFD) as a powerful numerical tool for flow prediction has been commonly used in reactor performance prediction and optimization[7–9]. Compared to UV disinfection, VUV/UV treatment, which incorporates advanced oxidation processes (AOPs) involving the generation and transport of highly reactive oxidizing radicals, imposes stricter demands on flow prediction. Many researchers have employed integral approaches to contaminants degradation simulation which are integrated CFD models, UV fluence distribution, photochemical models with consideration of several complex reaction pathways within the water matrix involving highly reactive free radicals such as hydroxyl radicals. Many previous studies were regard the degradation of poly-contaminant as the performance of VUV reactors. Bagheri and Mohseni[10–12] have developed a CFD modelling of VUV/UV photoreactors for the contaminant pCBA and utilized in the pilot reactor simulation. However, they are in despite of the oxidation by-products and the generation of secondary organic contaminants in the processes. Ouyang et al.[13] have studied the mineralization pathway and VUV/UV oxidation performance of aldehydes however in the bulk solutions. Due to the high flow rate requirements and the compact volume of the reactor, fluid in the reactor is predominantly in a turbulent state and the choice of turbulence model plays a critical role in pollutant degradation simulations. Liu et al.[14] demonstrated that the performance efficiency of disinfection reactors is highly dependent on the selection of the RANS turbulence model. However, most reported studies have not

focused on the influence of the turbulence model selection on the chemical reaction processes and transport of free radicals, especially in the compact UV reactors with complex flow pattern.

In this study, a CFD model that comprehensively account for the behaviours of the target contaminant in the reactor, including the distribution of VUV and high-reactive free radical, the degradation behaviours, the flow hydrodynamics, and the spatial concentration distribution of the total organic carbon, has been developed. Meanwhile, five RANS turbulence closures were utilized in the VUV/UV system simulation to investigate the influence of the turbulence model selection on the degradation of microcontaminants. The resulting hydraulic behaviours, fluence distribution, and microcontaminant transport dynamics were evaluated, providing valuable insights into reactor performance under different turbulence models.

2. CFD MODEL DEVELOPMENT

2.1. Reactor configurations

VUV/UV reactors are typically constructed by low pressure mercury lamp (which emits 254nm and 185nm ultraviolet), quartz sleeve and reactor body. Fig. 1 illustrates the configuration of the VUV/UV system featuring 45° angled inlet and outlet piping. The length of reaction region is 485.5mm and the diameter of inlet and outlet is 34.8mm. The internal diameter of the reactor is 42 mm. The lamp and quartz sleeve are centrally positioned within the reactor, with the lamp housed inside the quartz sleeve. The inner and outer diameter of the quartz are 21.6mm and 25mm and the length of the lamp is 483mm.

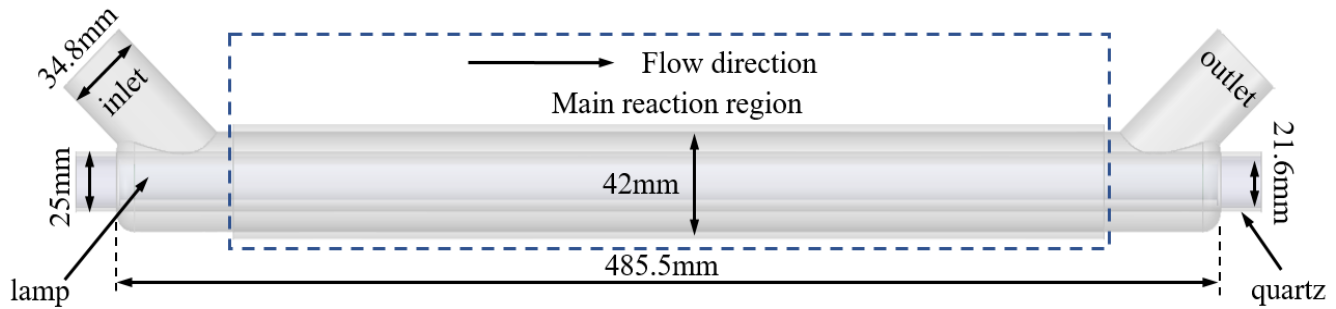


Fig. 1: The configuration of the VUV/UV system.

2.2. Hydrodynamic model

Assuming that the water acts as the Newtonian, incompressible, and isothermal fluid, characterized by steady-state flow with constant thermophysical properties. The Reynolds-averaged Navier–Stokes (RANS) equations using in the computational fluid dynamics (CFD) model can be written in Cartesian tensor form as continuity and momentum equations:

$$\frac{\partial}{\partial x_i} (\rho \bar{u}_i) = 0 \quad (1)$$

$$\frac{\partial}{\partial x_j} (\rho \bar{u}_i \bar{u}_j) = -\frac{\partial \bar{P}}{\partial x_i} + \rho g_i + \frac{\partial}{\partial x_j} \left[\mu \left(\frac{\partial \bar{u}_i}{\partial x_j} + \frac{\partial \bar{u}_j}{\partial x_i} - \rho \overline{u_i' u_j'} \right) \right] \quad (2)$$

where ρ is the fluid density, \bar{P} is the pressure, g_i is the gravitational acceleration in the i direction, \bar{u} is the fluid velocity, μ is the dynamic viscosity, $-\rho \overline{u_i' u_j'}$ refers to the turbulent stress and here u' is the turbulent fluctuations of velocity. The Boussinesq hypothesis is formulated as the following manner to ensure the closure of the equations for the $k - \epsilon$ models and $k - \omega$ models[15, 16]:

$$-\overline{\rho u_i' u_j'} = \mu_t \left(\frac{\partial \bar{u}_i}{\partial x_j} + \frac{\partial \bar{u}_j}{\partial x_i} \right) - \frac{2}{3} (\rho k + \mu_t \frac{\partial u_k}{\partial x_k}) \delta_{ij} \quad (3)$$

Three $k - \varepsilon$ models, including the standard, Re-normalization Group (RNG), and realizable $k - \varepsilon$ models, and two $k - \omega$ models, including the standard and Shear-stress transport (SST) $k - \omega$ models, are utilized in solving the turbulent viscosity.

Species conservation equation is introduced to predict the local mass fraction of Y_i of each specie:

$$\frac{\partial}{\partial x_j} (\rho u_j Y_i) = -\frac{\partial J_i}{\partial x_j} + R_i \quad (4)$$

The diffusive flux of species i in the turbulent flow can be estimated as follow:

$$J_i = -(\rho D_{i,m} + \frac{\mu_t}{Sc_t}) \frac{\partial Y_i}{\partial x_j} \quad (5)$$

where R_i is the net reaction rate, $D_{i,m}$ is molecular diffusivity of species and Sc_t is the Schmidt number.

2.3. Fluence model

The fluence rate field is computed by using the non-gray discrete ordinates (DO) model, which accounts for the integration of the radiative transfer equation (RTE) across individual wavelength intervals. The surface emission model is employed and the reflection, refraction, and absorption of photons propagating in different medium are incorporated in the radiation model. The RTE is expressed as:

$$\nabla \cdot (I_\lambda(\vec{r}, \vec{s}) \vec{s}) + (a_\lambda + \sigma_s) I_\lambda(\vec{r}, \vec{s}) = a_\lambda n^2 \frac{\sigma T^4}{\pi} + \frac{\sigma_s}{4\pi} \int_0^{4\pi} I_\lambda(\vec{r}, \vec{s}') \Phi(\vec{r}, \vec{s}') d\Omega' \quad (6)$$

where λ is wavelength, $I_\lambda(\vec{r}, \vec{s})$ is the spectral intensity associated with the position vector \vec{r} and the direction vector \vec{s} , a_λ is the spectral absorption coefficient, σ_s is the scattering coefficient, n is the refractive index, σ is the Stefan–Boltzmann constant, Φ is the phase function and Ω' is the solid angle of the scattering direction vector \vec{s}' .

2.4. Kinetic model

Two main degradation pathways of microcontaminants in the VUV/UV AOPs: direct photolysis and radical oxidation. For the target micropollutant M:



The rate of degradation of the compound M by photolysis and $OH \cdot$ radical oxidation can be expressed as:

$$r_M = -\ln(10) \Phi_M \varepsilon_M C_M E'_p(x) - k_M C_M C_{OH \cdot} \quad (9)$$

where Φ_M , ε_M , C_M and k_M respectively represents the quantum yield, molar absorption, concentration and radical reaction constant of the compound M, E'_p is the fluence rate and $C_{OH \cdot}$ is the concentration of the $OH \cdot$ radical.

2.5. Simulation setting

All governing equations were discretized using the finite volume method and solved using ANSYS® 20.2 fluent with the segregated steady-state solver. 2.8 million unstructured meshes were discretized using poly-hexahedral cells, with the boundary layer mesh constructed on the reactor walls and quartz sleeve surface to accurately capture near-wall flow characteristics and high concentration gradients. The lamp power was 70W (54W for 254nm output and 11W for 185nm output). The concentration of the model contaminant (acetaldehyde) and dissolved oxygen at inlet was set at 100ppb respectively. The degradation and mineralization pathways of acetaldehyde in the water matrix are integrated by the User Defined Function[17–22]. Due to the low concentration of the contaminant, assuming that there is negligible impact on the fluid quality. UV transmission of water and quartz were defined as 98% and 80% respectively, the absorption of water and air for 185nm VUV were set at 1.5 (/cm) and 0.166 (/cm). A mass flow rate of 0.64 kg/s, directed normally to the boundary, was established at the inlet, while a fully developed outflow condition was applied at the outlet. A no-slip boundary condition and zero diffusive flux for species were imposed on the walls. The lamp surface and quartz sleeve surface were modelled as semi-transparent, fully specular walls. The reactor wall was set as opaque wall, with purely reflectivity of 0.8.

In this study, the RANS approach with the standard, RNG and realizable $k - \varepsilon$ models, as well as the standard and SST $k - \omega$ models was used for comparisons. The Coupled algorithm was chosen for the pressure–velocity coupling and the least-squares approach was used for cell gradient calculation. Second order upwind discretization scheme was applied except for turbulent terms for which the first order upwind scheme was selected. The radiative transfer equation was solved by using the non-grey discrete ordinates (DO) model. Both the theta and phi divisions and the theta and phi pixels were set as 4×4 .

3. Result and discussion

Five RANS turbulence closures are employed in the VUV/UV system simulation for calculating flow hydrodynamics using the Coupled algorithm, as shown in Fig. 2. Differences are observed only at the corner of the reactor, where has the large turbulent kinetic energy and vortex generation. The computational results demonstrate that, for this reactor configuration, the selection of RANS models exposes a limited influence on velocity profile calculations, which subsequently has an insignificant effect on the contaminants distribution at the photoreactor outlet.

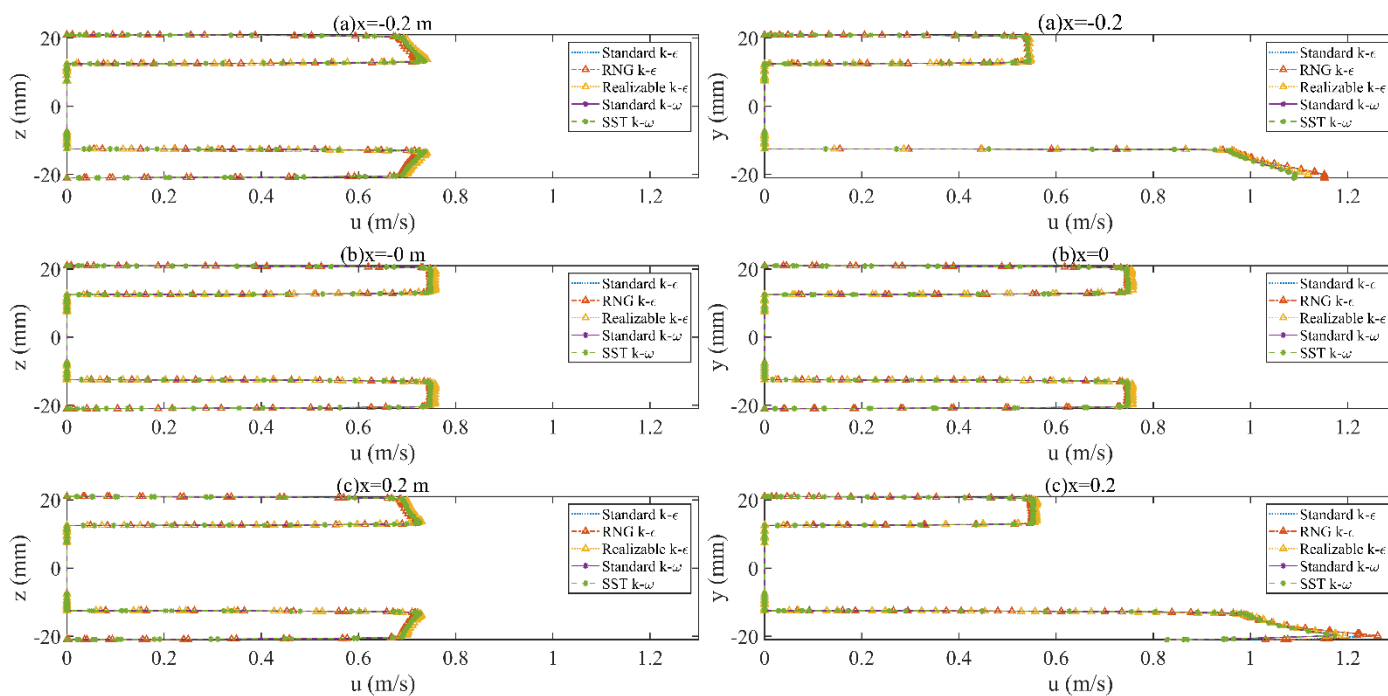


Fig. 2: Velocity profiles calculated by different turbulent models

Fig. 3 - Fig. 5 present the CFD results that comprehensively account for the behaviours of the target contaminant in the reactor, including the distribution of VUV and high-reactive free radical, the degradation behaviours, the flow hydrodynamics, and the spatial concentration distribution of the total organic carbon.

Fig. 3 depicts the strong positive correlation between the 185 nm VUV irradiance distribution and the concentration of highly reactive free radicals, specifically $OH \cdot$ radical. The data reveal that 185 nm VUV irradiation plays the essential role in the generation of $OH \cdot$ radical. Due to the significant absorption of VUV in the water matrix, the irradiance dramatically diminishes as the radiance exits from the quartz sleeve surface. Consequently, the highest concentration of $OH \cdot$ radicals is localized near the quartz surface, resulting in a prominent radial gradient and an uneven distribution of free radicals.

Fig. 4 illustrates the degradation behaviours of the target contaminant (acetaldehyde) within the continuous flow reactor. Previous studies [13] have investigated the mineralization pathway and VUV/UV oxidation performance of aldehydes in bulk solutions along the light-path. In Fig. 4, the stacked bar chart shows the concentration of the target

contaminant and secondary organic contaminants at different positions along the reactor flow channel, quantifying the oxidation performance throughout the reactor. The concentration of acetaldehyde decreases dramatically as it enters the reactor from the inlet and it is almost completely degraded at $x=0\text{m}$ (at the middle position of the reactor). This demonstrates the high sensitivity of target contaminant to VUV/UV oxidation and indicates that secondary organic contaminants have become the dominant form during the continues oxidation process. A slight increase in the concentration of total organic carbon can be observed from $x=-0.195\text{m}$ to $x=-0.15\text{m}$. This may be due to the generation of secondary organic contaminants from the oxidation by-products of acetaldehyde. The acetaldehyde is converted to more persistent carboxylic acids, predominantly formic and acetic acids, and consequently the mineralization of acetaldehyde becomes inefficient.

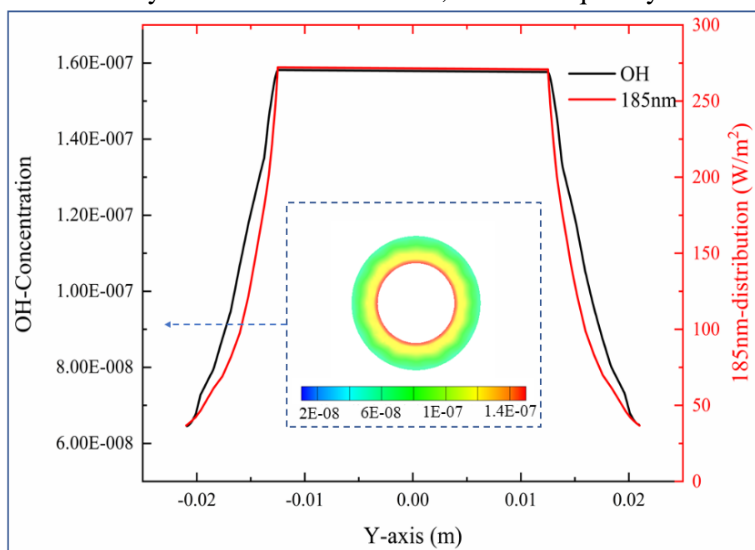


Fig. 3: The distribution of $\text{OH}\cdot$ and VUV.

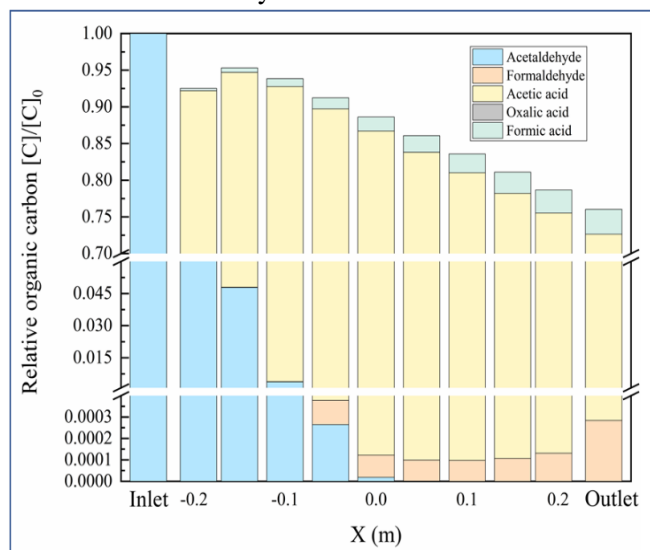


Fig. 4: The degradation behaviors of target contaminant.

Fig. 5 demonstrates the velocity profiles of flow and spatial concentration distribution of the total organic carbon. Fig. 5 (a) displays the velocity profiles at three cross-sections (at $x=-0.195\text{m}$, $x=0\text{m}$ and $x=0.195\text{m}$) calculated using the SST $k - \omega$ model, which illustrate the flow development along the reactor. Upon entering the reactor from the inlet, the flow encounters the corner between the inlet piping and the reactor channel. This leads to a higher velocity in the upper half of reactor ($y < 0$) compared to other regions, with the maximum velocity observed at the top of corner. Meanwhile, under the influence of gravity, the fluid flows downward and forward around the quartz sleeve, resulting in a relatively uniform velocity distribution along the z -axis. As a result, positions farther from the inlet show lower velocity. As the flow develops, the fluid rotates around the quartz sleeve, forming a uniform velocity profile at $x=0\text{m}$. At $x=0.195\text{m}$, the velocity profile resembles that at $x=-0.195\text{m}$ due to structural symmetry.

Fig. 5 (b) – (d) displays the spatial concentration distribution of the total organic carbon in the reactor. The flow with high concentration of contaminants enters from the inlet and undergoes oxidation along the reactor length. As observed in Fig. 5 (b) and Fig. 5 (c), the concentration near the reactor wall is obviously higher than that in the main reaction regions. This phenomenon is attributed to the gradient distribution of VUV irradiance and $\text{OH}\cdot$ radical concentration, as demonstrated in Fig. 3. Fig. 5 (c) shows that the contaminants in the half region ($y > 0$) has effectively oxidized because of the lower average velocity magnitude, which allows the prolonged exposure in VUV irradiance and interaction with highly reactive radicals. Fig. 5 (d) compares the radical distribution of contaminants concentration at three cross-sections (at $x=-0.195\text{m}$, $x=0\text{m}$ and $x=0.195\text{m}$). At $x=-0.195\text{m}$, the flow enters the reactor initially and the target contaminant is degraded immediately by contacting with the $\text{OH}\cdot$ radical. The vortex generated near the corner enhances mass transport and mixing, resulting in high degradation rates in the adjacent region. And as the fluid flows downward, secondary organic contaminants are generated by oxidation by-products of acetaldehyde, resulting in higher concentrations in the region ($y > 0$). As the flow develops along

the reactor, the concentration distribution at $x = 0$ m and $x = 0.195$ m becomes the opposite of that at $x = -0.195$ m, due to the lower velocity in the lower region ($y > 0$). At the outlet, the reactor demonstrates excellent performance in terms of acetaldehyde removal, as the acetaldehyde concentration is nearly zero. However, the acetaldehyde has been converted into more recalcitrant carboxylic acids, resulting in only 24.0% reduction of the total organic carbon at the outlet.

4. Conclusion

This study presents a CFD model that comprehensively account for the behaviours of the target contaminant in the reactor, including distribution of VUV and high-reactive free radical, degradation and formation behaviour of primary and secondary pollutants, flow hydrodynamics, and the spatial concentration distribution of the total organic carbon. Five RANS closures

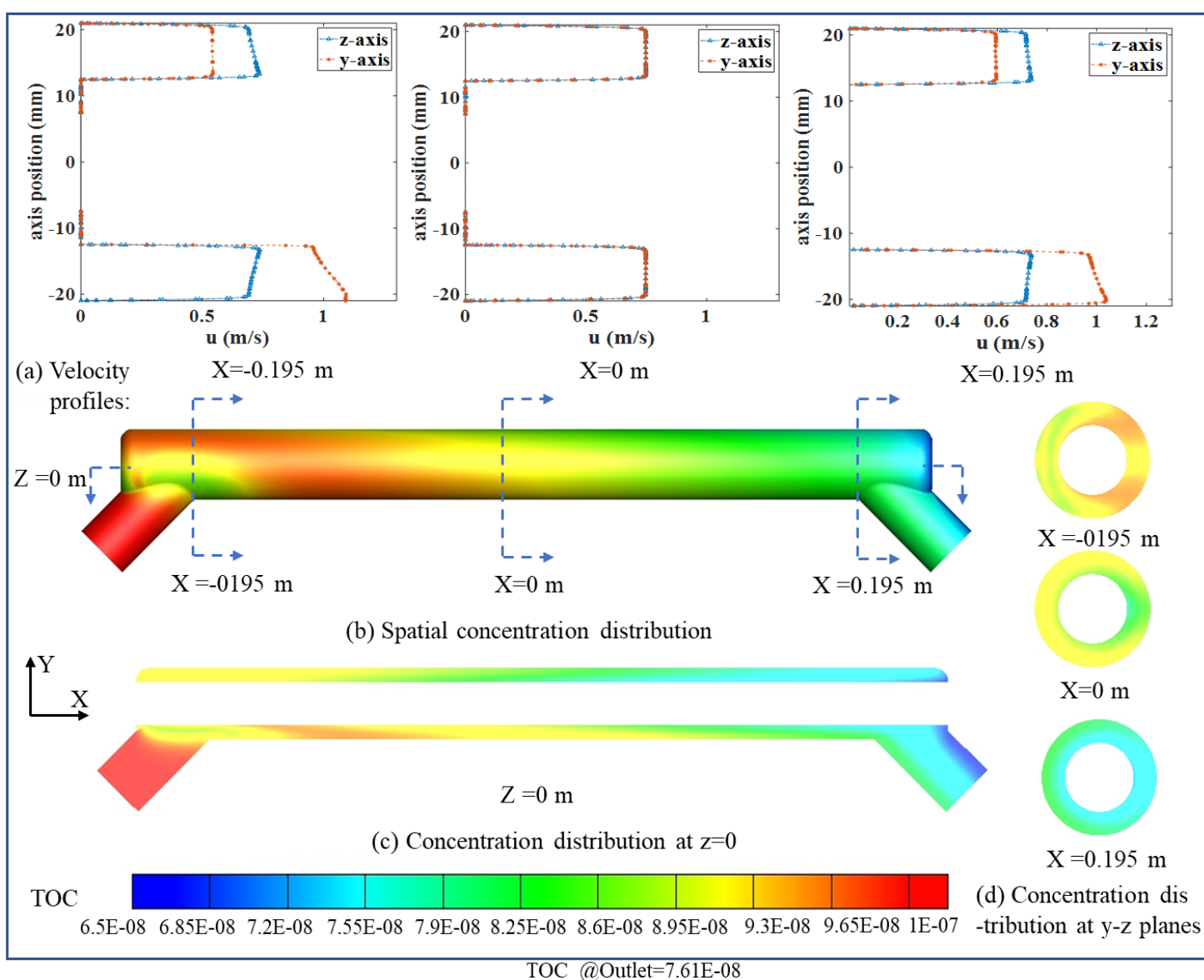


Fig. 5: The velocity profiles and spatial concentration distribution.

used for calculating flow hydrodynamics reveal the difference only at the corner of the reactor where has the large turbulent kinetic energy, while exposing negligible influence on the pollutant distribution at the outlet.

Results indicate a strong positive correlation between 185 nm VUV irradiance and OH· radical generation. The sensitivity of primary and secondary contaminants to VUV light and highly reactive free radicals significantly influences the performance of the photoreactor. The hydrodynamics and internal mass transfer within the reactor influence the spatial distribution of reactants inside the photoreactor.

Acknowledgements

This research was supported by the National Natural Science Foundation of China No. 52450231, and Zhejiang Provincial Natural Science Foundation of China under Grant No. LD24E050008.

References

- [1] R. Singh, "Development of Hybrid Processes for High Purity Water Production," in *Emerging Membrane Technology for Sustainable Water Treatment*, Elsevier, 2016, pp. 327–357.
- [2] P. Zhao, Y. Bai, B. Liu, H. Chang, Y. Cao, and J. Fang, "Process optimization for producing ultrapure water with high resistivity and low total organic carbon," *Process Safety and Environmental Protection*, vol. 126, pp. 232–241, 2019.
- [3] H. Lee, Y. Jin, and S. Hong, "Recent transitions in ultrapure water (UPW) technology: Rising role of reverse osmosis (RO)," *Desalination*, vol. 399, pp. 185–197, 2016.
- [4] K. G. Linden, N. Hull, and V. Speight, "Thinking Outside the Treatment Plant: UV for Water Distribution System Disinfection," *Acc. Chem. Res.*, vol. 52, no. 5, pp. 1226–1233, 2019.
- [5] H. M. Coleman, V. Vimonses, G. Leslie, and R. Amal, "Degradation of 1,4-dioxane in water using TiO₂ based photocatalytic and H₂O₂/UV processes," *Journal of Hazardous Materials*, vol. 146, no. 3, pp. 496–501, 2007.
- [6] X. Zhang, Y. Yang, H. Ngo, W. Guo, H. Wen, X. Wang, J. Zhang, T. Long, "A critical review on challenges and trend of ultrapure water production process," *Science of The Total Environment*, vol. 785, p. 147254, 2021.
- [7] J. Zhang, A. E. Tejada-Martínez, and Q. Zhang, "Developments in computational fluid dynamics-based modeling for disinfection technologies over the last two decades: A review," *Environ Modell Softw*, vol. 58, pp. 71–85, 2014.
- [8] J. Shah, A. Židonis, and G. Aggidis, "State of the art of UV water treatment technologies and hydraulic design optimisation using computational modelling," *J Water Process Eng*, vol. 41, p. 102099, 2021.
- [9] S. I. Ngo and Y.-I. Lim, "Multiscale eulerian CFD of chemical processes: A review," *ChemEngineering*, vol. 4, no. 2, p. 23, 2020.
- [10] M. Bagheri and M. Mohseni, "Computational fluid dynamics (CFD) modeling of VUV/UV photoreactors for water treatment," *Chem Eng J*, vol. 256, pp. 51–60, 2014.
- [11] M. Bagheri and M. Mohseni, "Impact of hydrodynamics on pollutant degradation and energy efficiency of VUV/UV and H₂O₂/UV oxidation processes," *J Environ Manage*, vol. 164, pp. 114–120, 2015.
- [12] M. Bagheri and M. Mohseni, "Pilot-scale treatment of 1,4-dioxane contaminated waters using 185 nm radiation: Experimental and CFD modeling," *J Water Process Eng*, vol. 19, pp. 185–192, 2017.
- [13] W.-Y. Ouyang, W.-L. Wang, Y.-L. Zhang, H.-Y. Cai, and Q.-Y. Wu, "VUV/UV oxidation performance for the elimination of recalcitrant aldehydes in water and its variation along the light-path," *Water Research*, vol. 228, p. 119390, 2023.
- [14] D. Liu, C. Wu, K. Linden, and J. Ducoste, "Numerical simulation of UV disinfection reactors: Evaluation of alternative turbulence models," *Applied Mathematical Modelling*, vol. 31, no. 9, pp. 1753–1769, 2007.
- [15] Y. Cao, R. Xu, and P. Jiang, "Physics-informed machine learning based RANS turbulence modeling convection heat transfer of supercritical pressure fluid," *International Journal of Heat and Mass Transfer*, vol. 201, p. 123622, 2023.
- [16] J. Wu, B. Deng, X. Zou, and J. Luo, "A systematic simulation of disinfection for the flow-through UV reactors with staggered ring baffles under the Eulerian framework," *Journal of Water Process Engineering*, vol. 52, p. 103598, 2023.

- [17]G. V. Buxton, C. L. Greenstock, W. P. Helman, and A. B. Ross, "Critical Review of rate constants for reactions of hydrated electrons, hydrogen atoms and hydroxyl radicals ($\cdot\text{OH}/\cdot\text{O}^-$ in Aqueous Solution)," *Journal of Physical and Chemical Reference Data*, vol. 17, no. 2, pp. 513–886, 1988.
- [18]J. C. Crittenden, S. Hu, D. W. Hand, and S. A. Green, "A kinetic model for H₂O₂/UV process in a completely mixed batch reactor," *Water Research*, vol. 33, no. 10, pp. 2315–2328, 1999.
- [19]G. Imoberdorf and M. Mohseni, "Modeling and experimental evaluation of vacuum-UV photoreactors for water treatment," *CHEMICAL ENGINEERING SCIENCE*, vol. 66, no. 6, pp. 1159–1167, 2011.
- [20]J. Li, Q. Zhang, B. Chen, L. Wang, R. Zhu, and J. Yang, "Hydrogen peroxide formation in water during the VUV/UV irradiation process: Impacts and mechanisms of selected anions," *Environmental Research*, vol. 195, p. 110751, 2021.
- [21]M. I. Stefan, A. R. Hoy, and J. R. Bolton, "Kinetics and Mechanism of the Degradation and Mineralization of Acetone in Dilute Aqueous Solution Sensitized by the UV Photolysis of Hydrogen Peroxide," *Environ. Sci. Technol.*, vol. 30, no. 7, pp. 2382–2390, 1996.
- [22]T. Zhang and C.-H. Huang, "Modeling the Kinetics of UV/Peracetic Acid Advanced Oxidation Process," *Environ. Sci. Technol.*, vol. 54, no. 12, pp. 7579–7590, 2020.